JOURNAL OF GEOPHYSICAL RESEARCH, VOL. 100, NO. C12, PAGES 24,863–24,872, DECEMBER 15, 1995

Generation and propagation of infragravity waves

T. H. C. Herbers
Department of Oceanography, Naval Postgraduate School, Monterey, California

Steve Elgar
School of Electrical Engineering and Computer Science, Washington State University, Pullman

R. T. Guza
Center for Coastal Studies, Scripps Institution of Oceanography, La Jolla, California

Abstract. The generation and propagation of infragravity waves (frequencies nominally 0.004–0.04 Hz) are investigated with data from a 24-element, coherent array of pressure sensors deployed for 9 months in 13-m depth, 2 km from shore. The high correlation between observed ratios of upcoast to downcoast energy fluxes in the infragravity ($F_{up}^{IG}/F_{down}^{IG}$) and swell ($F_{up}^{swell}/F_{down}^{swell}$) frequency bands indicates that the directional properties of infragravity waves are strongly dependent on incident swell propagation directions. However, $F_{up}^{IG}/F_{down}^{IG}$ is usually much closer to 1 (i.e., comparable upcoast and downcoast fluxes) than is $F_{up}^{swell}/F_{down}^{swell}$, suggesting that upcoast propagating swell drives both upcoast and downcoast propagating infragravity waves. These observations agree well with predictions of a spectral WKB model based on the long-standing hypothesis that infragravity waves, forced by nonlinear interactions of nonbreaking, shoreward propagating swell, are released as free waves in the surf zone and subsequently reflect from the beach. The radiated free infragravity waves are predicted to be directionally broad and predominantly refractively trapped on a gently sloping shelf. The observed ratios $F_{sea}^{IG}/F_{shore}^{IG}$ of the seaward and shoreward infragravity energy fluxes are indeed scattered about the theoretical value 1 for trapped waves when the swell energy is moderate, but the ratios deviate significantly from 1 with both low- and high-energy swell. Directionally narrow, shoreward propagating infragravity waves, observed with low-energy swell, likely have a remote (possibly trans-oceanic) energy source. High values (up to 5) of $F_{sea}^{IG}/F_{shore}^{IG}$, observed with high-energy swell, suggest that high-mode edge waves generated near the shore can be suppressed by nonlinear dissipation processes (e.g., bottom friction) on the shelf.

1. Introduction

Infragravity waves, motions with periods of nominally 0.4–4 min, are believed important to harbor oscillations, sediment transport, and other nearshore processes. A strong correlation between the energy levels of infragravity waves and swell indicates that infragravity waves are driven by swell (*Munk* [1949], *Tucker* [1950], and many others). *Longuet-Higgins and Stewart* [1962] suggested that while the incident swell is dissipated by breaking in very shallow water, the associated infragravity-frequency second-order forced waves (excited by nonlinear difference-frequency interactions of pairs of swell components) are somehow released as free waves and reflect from the beach. These seaward propagating free waves may reflect back toward shore from a turning point on the sloping beach or shelf (i.e., edge waves) or radiate into deep ocean basins (i.e., leaky waves). Idealized models were subsequently developed for the resonant excitation of edge waves by nonlinear difference-frequency interactions of pairs of obliquely incident swell components [e.g., *Gallagher*, 1971; *Foda and Mei*, 1981]. Wave breaking was neglected in *Gallagher*'s [1971] model, but laboratory experiments with wave breaking nonetheless exhibit the gross properties of the predicted edge wave excitation [*Bowen and Guza*, 1978]. *Symonds et al.* [1982] subsequently showed that slow oscillations in the wave setup (associated with slow variations of the breakpoint location of groupy incident swell) can also drive infragravity waves. This mechanism, which requires wave breaking, has been heuristically incorporated in models for infragravity wave generation by normally incident waves [e.g., *List*, 1992; *Schäffer*, 1993]. Existing infragravity wave generation models are not generally applicable to the random and directionally spread wave fields observed on natural beaches, and detailed quantitative comparisons with field data have not been reported. The effect of wave breaking on resonant nonlinear wave interactions and the relative importance of breaking-wave-induced setup variations to infragravity wave generation are still poorly understood.

Infragravity motions observed on the continental shelf in depths ranging from 8 to 200 m are a mixture of forced waves that are accurately predicted by second-order nonlinear wave theory [*Herbers et al.*, 1994] and (usually more energetic) free waves radiated from shore [*Herbers et al.*, 1995, and references therein]. In the present study, the generation and propagation of free infragravity waves is further investigated with data from a 250 m × 250 m aperture array of 24 bottom-mounted pres-

Paper number 95JC02680.
0148-0227/95/95JC-02680$05.00

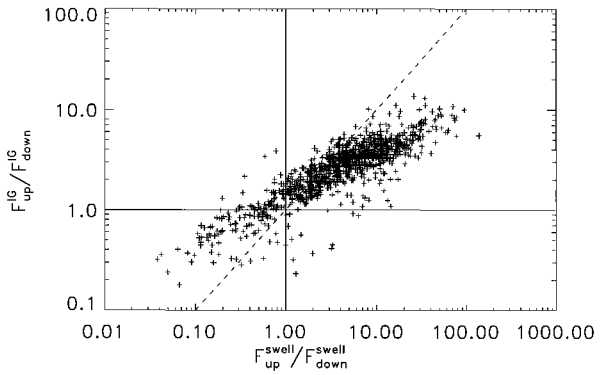

Figure 1. The ratio $F_{up}^{IG}/F_{down}^{IG}$ of the upcoast to the downcoast component of the alongshore energy flux in the infragravity frequency band versus the analogous flux ratio $F_{up}^{swell}/F_{down}^{swell}$ in the swell frequency band. The dashed line corresponds to equal ratios.

sure transducers, deployed for 9 months in 13-m depth on a gently sloping beach near Duck, North Carolina (see *Herbers et al.* [1994] for a detailed description of the experiment). The array was situated 2 km from shore, well offshore of the turning points of low-mode edge waves [*Ursell*, 1952] that may dominate the infragravity band inside the surf zone [e.g., *Huntley et al.*, 1981; *Oltman-Shay and Guza*, 1987].

The observed relative contributions of upcoast and downcoast traveling waves to the alongshore infragravity wave energy flux are shown in section 2 to depend strongly on incident swell propagation directions and to compare favorably with predictions of a simple model [after *Longuet-Higgins and Stewart*, 1962] for the directional properties of infragravity waves radiated from shore. The model incorporates second-order finite depth theory [*Hasselmann*, 1962] for infragravity wave generation by swell interactions in shallow water shoreward of the array, and a WKB approximation for the spectral transformation of shoaling incident swell and seaward radiated infragravity waves. Because very little is known about the breaking of natural, directionally spread, incident waves, surf zone forcing and dissipation effects were not included in the infragravity wave predictions. Cross-shore fluxes of energy are discussed in section 3. WKB theory predicts that the directionally broad infragravity wave field radiated from shore is predominantly refractively trapped on the continental shelf. The observed ratios between the seaward and shoreward components of the cross-shore infragravity wave energy flux are scattered about the theoretical value 1 for inviscid trapped waves. However, observed systematic deviations from 1 suggest that high-mode edge waves on the shelf are damped in the presence of energetic swell and that remotely generated waves contribute significantly to the infragravity band when local swell energy levels are relatively low. The results are summarized in section 4.

2. Alongshore Energy Fluxes

2.1. Observations

Previous analysis of a few array data records [*Herbers et al.*, 1995] showed that the directional spectrum of infragravity waves is usually broad and sensitive to incident swell propagation directions. This dependence is further explored here using a more quantitative analysis of the entire data set. Bulk directional properties of infragravity waves and swell were estimated from the array measurements using a technique [*Elgar et al.*, 1994] that assumes the linear dispersion relation (equation (A1)). This assumption is justified in Appendix A. The relative contributions of upcoast and downcoast traveling waves to the alongshore wave energy flux density

$$F_{up}(f) = -\rho g c_g(f) \int_{-\pi}^{0} d\theta \sin\theta E(f, \theta) \tag{1a}$$

$$F_{down}(f) = \rho g c_g(f) \int_{0}^{\pi} d\theta \sin\theta E(f, \theta) \tag{1b}$$

where ρ is the density of seawater, g is gravity, c_g is group speed, and $E(f, \theta)$ is the frequency (f)–directional (θ) spectrum of surface elevation fluctuations ($\theta = 0$ corresponds to shoreward propagation), were estimated for each of the 840 three-hour long data records. Integration over frequency yields bulk upcoast and downcoast energy fluxes for the infragravity and swell bands:

$$F_{up}^{IG} = \int_{0.01\ Hz}^{0.04\ Hz} df\, F_{up}(f) \tag{2a}$$

$$F_{down}^{IG} = \int_{0.01\ Hz}^{0.04\ Hz} df\, F_{down}(f) \tag{2b}$$

$$F_{up}^{swell} = \int_{0.04\ Hz}^{0.14\ Hz} df\, F_{up}(f) \tag{2c}$$

$$F_{down}^{swell} = \int_{0.04\ Hz}^{0.14\ Hz} df\, F_{down}(f) \tag{2d}$$

where the 0.04-Hz cutoff frequency was conservatively chosen to avoid contamination of the infragravity band estimates by more energetic swell. Frequencies less than 0.01 Hz are not considered because the fluxes associated with these long-wavelength (>1 km) waves are not well estimated by the array.

The ratio $F_{up}^{IG}/F_{down}^{IG}$ between upcoast and downcoast infragravity energy fluxes depends on $F_{up}^{swell}/F_{down}^{swell}$, the analogous ratio in the swell band (Figure 1). As $F_{up}^{swell}/F_{down}^{swell}$ increases, $F_{up}^{IG}/F_{down}^{IG}$ increases, indicating that upcoast (downcoast) propagating swell drives predominantly upcoast (downcoast) propagating infragravity waves. However, the infragravity ratios are usually much closer to 1 (i.e., equal upcoast and downcoast fluxes) than are the swell ratios ($F_{up}^{IG}/F_{down}^{IG}$ ranges between about 0.2 and 10, whereas $F_{up}^{swell}/F_{down}^{swell}$ ranges between 0.04 and 100 (Figure 1)). These observations suggest the possible importance of backscattering of infragravity waves from topographic irregularities or the direct excitation of opposing alongshore infragravity energy fluxes by swell.

2.2. Model

Nonlinear interaction between a pair of swell components with frequencies and vector wavenumbers (f_1, $\mathbf{k}_1$) and (f_2, $\mathbf{k}_2$) theoretically forces a secondary (infragravity) wave with the difference frequency and wavenumber ($f_2 - f_1$, $\mathbf{k}_2 - \mathbf{k}_1$) (for $f_2 > f_1$). As the water depth h decreases, forced wave amplitudes increase rapidly (Figure 2a) because interactions involving a pair of swell components traveling in approximately the

same direction become nearly resonant (i.e., $(f_2 - f_1, |\mathbf{k}_2 - \mathbf{k}_1|)$ is close to the linear dispersion relation (equation (A1))). *Longuet-Higgins and Stewart* [1962] hypothesized that while swell energy is mostly dissipated in the surf zone, the associated longer-wavelength forced infragravity waves are released as free waves, reflect from the beach, and radiate seaward. The approximately $h^{-1/2}$ decrease in energy ("unshoaling") of an outgoing, leaky free wave is more gradual than the approximately h^{-5} amplification of an incoming forced wave. Free waves are thus expected to dominate the infragravity band well outside the surf zone, consistent with many observations [e.g., *Okihiro et al.*, 1992; *Elgar et al.*, 1992; *Herbers et al.*, 1995].

Interactions between swell components propagating directly onshore force onshore propagating infragravity waves. However, if the infragravity frequency $f_2 - f_1$ is small compared with the swell frequencies f_1, f_2, then $|\mathbf{k}_2 - \mathbf{k}_1| \ll |\mathbf{k}_1|, |\mathbf{k}_2|$ and even slight obliquity of the incident swell can yield an infragravity wave propagating at a grazing angle relative to the shoreline. The nonlinearly excited infragravity wave field is expected to be directionally broader than the incident swell and refractively trapped close to shore (Figure 2b and section 3).

The forced infragravity wave field excited by a spectrum of surface gravity waves in arbitrary water depth h follows from a perturbation expansion of the governing equations and boundary conditions to second order [*Hasselmann*, 1962]. The lowest-order velocity potential $\Phi^{(1)}$ is assumed to be a linear superposition of statistically independent swell components

$$\Phi^{(1)}(t, \mathbf{x}, z) = \int_{\mathbf{k}} dZ\,(\mathbf{k}) \exp\,[i(\mathbf{k}\cdot\mathbf{x} - \sigma t)] \cdot \frac{g \cosh\,[k(z+h)]}{i\sigma \cosh\,[k\ h]} + \mathrm{CC} \qquad (3)$$

where t is time, $\mathbf{x}$ $(=[x, y])$ and z are the horizontal and vertical (relative to the mean sea surface) space coordinates, dZ is the complex sea surface elevation amplitude function, the wavenumber k $(= |\mathbf{k}|)$ and radian frequency σ $(= 2\pi f)$ are related by the dispersion relation (equation (A1)), and CC or an asterisk indicates the complex conjugate.

Forced secondary waves at infragravity frequencies result from difference-frequency interactions of the primary swell components, and the secondary velocity potential $\Phi^{(2)}$ is given by (neglecting sum-frequency interactions)

$$\Phi^{(2)}(t, \mathbf{x}, z) = \int_{\mathbf{k}_1}\int_{\mathbf{k}_2} D(\mathbf{k}_1, \mathbf{k}_2)\, dZ^*\,(\mathbf{k}_1)\, dZ\,(\mathbf{k}_2) \cdot \exp\,[i\,[(\mathbf{k}_2 - \mathbf{k}_1)\cdot\mathbf{x} - (\sigma_2 - \sigma_1)t]] \cdot \frac{g \cosh\,[|\mathbf{k}_2 - \mathbf{k}_1|(z+h)]}{i(\sigma_2 - \sigma_1)\cosh\,[|\mathbf{k}_2 - \mathbf{k}_1|h]} + \mathrm{CC} \qquad (4)$$

with

$$D(\mathbf{k}_1, \mathbf{k}_2) = \frac{-(\sigma_2 - \sigma_1)^2}{g|\mathbf{k}_2 - \mathbf{k}_1| \tanh\,[|\mathbf{k}_2 - \mathbf{k}_1|h] - (\sigma_2 - \sigma_1)^2} \cdot \left\{ \frac{\sigma_1\sigma_2}{g} + \frac{g\mathbf{k}_1\cdot\mathbf{k}_2}{\sigma_1\sigma_2} - \frac{g}{2(\sigma_2 - \sigma_1)} \cdot \left[\frac{k_2^2}{\sigma_2 \cosh^2(k_2 h)} - \frac{k_1^2}{\sigma_1 \cosh^2(k_1 h)} \right] \right\} \qquad (5)$$

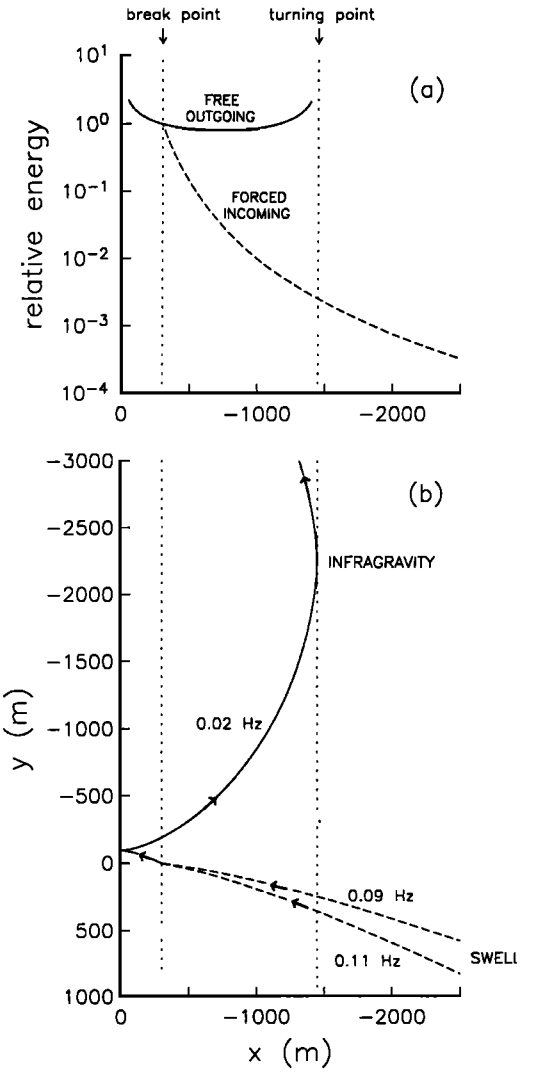

Figure 2. Schematic of infragravity wave generation on a plane beach (slope 0.01) by nonlinear interaction of two swell components with frequencies and deep water incidence angles of (0.09 Hz, −25°) and (0.11 Hz, −30°). The forced, shoreward propagating infragravity wave with the difference frequency 0.02 Hz is nearly resonant in shallow water and strongly amplified (Figure 2a, dashed line). While the incident swell components are dissipated through breaking, the forced infragravity wave is released as a free wave, reflects from the beach, and radiates seaward (Figure 2a, solid line). Well outside the surf zone the (weakly depth dependent) outgoing free wave is much more energetic than the incoming forced wave. Note that even for these moderately small angles of swell incidence (Figure 2b, dashed lines) the outgoing free infragravity wave is refractively trapped close to shore (Figure 2b, solid line).

A simple relationship between the asymptotic forced infragravity wave variance in shallow water E_{IG}

$$E_{IG} \equiv \mathbf{E}\left\{ \left| \frac{-1}{g} \frac{\partial \Phi^{(2)}}{\partial t} \right|^2 \right\} \qquad (6)$$

(where $\mathbf{E}\{\}$ indicates the expected value [see *Herbers et al.*, 1992]) and the deepwater incident swell spectrum is now derived for a mildly sloping beach with straight and parallel depth contours. The (double-sided) frequency–alongshore wavenumber spectrum of swell in shallow water $E(\sigma, k_y)$ in terms of the

deepwater spectrum $E_0(\sigma, k_y)$ follows from Snell's law [e.g., *Longuet-Higgins*, 1957]

$$E(\sigma, k_y) \equiv \frac{\mathbf{E}\{dZ(\mathbf{k})\, dZ^*(\mathbf{k})\}}{d\sigma dk_y} = \frac{g^{3/2}k_{x,0}}{2\sigma^3 h^{1/2}} E_0(\sigma, k_y) \qquad (7)$$

where $k_{x,0}$ is the deepwater cross-shore wavenumber. The corresponding shallow-water limit of the interaction coefficient D (equation 5) is [*Herbers et al.*, 1992]

$$D(\mathbf{k}_1, \mathbf{k}_2) = -\frac{3}{2}\frac{g}{\sigma_1\sigma_2 h^2}\left[1 + \left(\frac{(gk_{y2}/\sigma_2) - (gk_{y1}/\sigma_1)}{\sigma_2 - \sigma_1}\right)^2\right]^{-1} \qquad (8)$$

Substituting (4), (7), and (8) in (6) yields

$$E_{IG} = \int_{\sigma_{min}}^{\sigma_{max}} d\sigma_1 \int_{\sigma_1+\Delta\sigma_{min}}^{\sigma_1+\Delta\sigma_{max}} d\sigma_2 \int_{-\sigma_1^2/g}^{\sigma_1^2/g} dk_{y1} \int_{-\sigma_2^2/g}^{\sigma_2^2/g} dk_{y2} \cdot \frac{C(\sigma_1, \sigma_2, k_{y1}, k_{y2})}{h^5} E_0(\sigma_1, k_{y1})\, E_0(\sigma_2, k_{y2}) \qquad (9)$$

where $[\sigma_{min}, \sigma_{max}]$ and $[\Delta\sigma_{min}, \Delta\sigma_{max}]$ are the frequency ranges of the primary (swell) and secondary (infragravity) waves, respectively, and C is

$$C(\sigma_1, \sigma_2, k_{y1}, k_{y2}) = \frac{9}{2}\left(\frac{g}{\sigma_1\sigma_2}\right)^5 k_{x1,0}k_{x2,0} \cdot \left[1 + \left(\frac{(gk_{y2}/\sigma_2) - (gk_{y1}/\sigma_1)}{\sigma_2 - \sigma_1}\right)^2\right]^{-2} \qquad (10)$$

The predicted h^{-5} (equation (9)) growth of forced waves is invalid near the shoreline [*Longuet-Higgins and Stewart*, 1962]. However, the alongshore wavenumbers of both primary (k_{y1}), (k_{y2}) and secondary $(k_{y2} - k_{y1})$ waves are conserved, and in shallow water C is a function only of the frequencies and deepwater propagation directions of the primary wave components (equation (10)). Thus although in the shallow water limit the predicted forced infragravity wave energy is singular and is expected to be modified by the onset of wave breaking, the distribution of energy in (σ, k_y) space is depth-independent.

When forced infragravity waves are released as free waves and reflect from the beach, the alongshore wavenumber is also conserved. Hence the free infragravity waves radiated from shore have the same k_y energy distribution as the incoming forced infragravity waves, and certain directional properties of the radiated free waves are independent of the depth where the incoming forced waves are released. For example, the theoretical ratio between upcoast (F_{up}^{IG}) and downcoast (F_{down}^{IG}) energy fluxes (equation (2)) of free infragravity waves in asymptotically shallow water is obtained by weighting the expression for the released infragravity energy (equation (9)) by the alongshore component of the group velocity $c_{gy} = gh(k_{y2} - k_{y1})/(\sigma_2 - \sigma_1)$ and partitioning the integrals into upcoast $(k_{y2} - k_{y1} < 0)$ and downcoast $(k_{y2} - k_{y1} > 0)$ contributions

$$\frac{F_{up}^{IG}}{F_{down}^{IG}} = -\int_{\sigma_{min}}^{\sigma_{max}} d\sigma_1 \int_{\sigma_1+\Delta\sigma_{min}}^{\sigma_1+\Delta\sigma_{max}} d\sigma_2 \int_{-\sigma_1^2/g}^{\sigma_1^2/g} dk_{y1} \int_{-\sigma_2^2/g}^{k_{y1}} dk_{y2} \cdot \frac{k_{y2} - k_{y1}}{\sigma_2 - \sigma_1} C(\sigma_1, \sigma_2, k_{y1}, k_{y2}) E_0(\sigma_1, k_{y1}) E_0(\sigma_2, k_{y2})$$

$$\cdot \left(\int_{\sigma_{min}}^{\sigma_{max}} d\sigma_1 \int_{\sigma_1+\Delta\sigma_{min}}^{\sigma_1+\Delta\sigma_{max}} d\sigma_2 \int_{-\sigma_1^2/g}^{\sigma_1^2/g} dk_{y1} \int_{k_{y1}}^{\sigma_2^2/g} dk_{y2} \cdot \frac{k_{y2} - k_{y1}}{\sigma_2 - \sigma_1} C(\sigma_1, \sigma_2, k_{y1}, k_{y2}) E_0(\sigma_1, k_{y1}) E_0(\sigma_2, k_{y2})\right)^{-1} \qquad (11)$$

2.3. Model-Data Comparisons

Since both incident swell and associated infragravity waves were measured in intermediate (13 m) depth water, theoretical predictions of $F_{up}^{IG}/F_{down}^{IG}$ were obtained numerically with finite depth theory rather than the simple analytic asymptotic relationship (equation (11)). As is detailed in Appendix B, the measured frequency-directional spectrum of swell in 13-m depth was transformed to shallow water with linear shoaling and refraction theory. Second-order finite depth theory was then applied to the shallow water swell spectrum to predict the frequency-directional spectrum of forced shoreward propagating infragravity waves. This forced wave spectrum was subsequently reflected from the beach and transformed back to the 13 m depth array, accounting for unshoaling, refraction, and trapping effects with a WKB approximation. Finally, the flux ratio $F_{up}^{IG}/F_{down}^{IG}$ in 13-m depth was calculated from the predicted frequency-directional spectrum with (1) and (2a)–(2b).

Although the predicted $F_{up}^{IG}/F_{down}^{IG}$ ratios exclude low mode edge waves trapped shoreward of the array and are insensitive to contributions of leaky waves radiated to the deep ocean (i.e., small values of sin θ in (1)), the effect of variable damping of waves trapped on the shelf seaward of the array is neglected. That is, infragravity waves propagating seaward at large oblique angles may be strongly amplified by multiple reflections between the shoreline and caustics on the inner shelf (seaward of the array), whereas waves radiated at smaller oblique angles may be significantly damped before reaching a turning point on the outer shelf. These possibly strong variations in the amplification of high-mode edge waves are not accounted for in the model predictions (infragravity wave damping and radiation are further discussed in section 3). Although the model is qualitative, the observed and predicted $F_{up}^{IG}/F_{down}^{IG}$ ratios nonetheless agree within about a factor of 2 for the 20 cases examined here (Figure 3). The good agreement between observed and predicted ratios of upcoast and downcoast infragravity energy fluxes strongly supports the hypothesis that quadratic nonlinear interactions of swell drive free infragravity waves and further suggests that the directional properties of infragravity waves observed well outside the surf zone may be accurately predicted by a model that neglects wave-breaking effects.

2.4. Discussion

The dependence of the infragravity wave field on incident swell propagation directions in general, and in particular the generation of opposing alongshore energy fluxes suggested by the observations (Figure 1), is clarified by recasting (9) and (10) in terms of $E_0(\sigma, \theta_0)$, the frequency-directional spectrum of incident swell in deep water

$$E_{IG} = \int_{\sigma_{min}}^{\sigma_{max}} d\sigma_1 \int_{\sigma_1+\Delta\sigma_{min}}^{\sigma_1+\Delta\sigma_{max}} d\sigma_2 \int_{-\pi/2}^{\pi/2} d\theta_{1,0} \int_{-\pi/2}^{\pi/2} d\theta_{2,0}$$

$$\cdot \frac{C(\sigma_1, \sigma_2, \theta_{1,0}, \theta_{2,0})}{h^5} E_0(\sigma_1, \theta_{1,0}) E_0(\sigma_2, \theta_{2,0}) \quad (12)$$

with

$$C(\sigma_1, \sigma_2, \theta_{1,0}, \theta_{2,0}) = \frac{9}{2}\left(\frac{g}{\sigma_1\sigma_2}\right)^3 \cos\theta_{1,0} \cos\theta_{2,0}$$

$$\cdot \left[1 + \left(\frac{\sigma_2 \sin\theta_{2,0} - \sigma_1 \sin\theta_{1,0}}{\sigma_2 - \sigma_1}\right)^2\right]^{-2} \quad (13)$$

The predicted infragravity energy is sensitive to the frequencies of the interacting incident waves. For example, infragravity waves forced by two normally incident swell components with frequencies $f_1 = 0.09$ and $f_2 = 0.11$ Hz, are 65 times more energetic than infragravity waves forced by equally energetic, but higher-frequency ($f_1 = 0.19$, $f_2 = 0.21$ Hz) normally incident seas. This strong frequency dependence of the infragravity response is consistent with many observations [*Elgar et al.*, 1992, and references therein]. The more complicated dependence of infragravity energy levels on incident swell propagation directions is illustrated in Figure 4a for fixed swell frequencies of 0.09 and 0.11 Hz. The interaction coefficient C is maximum ($C_{max} = [9g^3]/[2\sigma_1^3\sigma_2^3]$) for colinear and normally incident swells ($\theta_{1,0} = 0$ and $\theta_{2,0} = 0$ in Figure 4a). However, C is not greatly reduced by moderately large swell-incidence and swell-spreading angles. The maximum infragravity response to obliquely incident swell ($C = C_{max} \cos\theta_{1,0} \cos\theta_{2,0}$) occurs at the nonzero deepwater spreading angle $\sigma_1 \sin\theta_{1,0} = \sigma_2 \sin\theta_{2,0}$ for which the refracted propagation directions in shallow water are colinear and therefore closest to resonance (equation (13)). For this small spreading angle, even deepwater swell incidence angles of 45° cause only about a factor of 2 reduction in C (from C_{max}). Similarly, moderately large spreading angles do not markedly reduce C. For example, for $\theta_{1,0} = -30°$, there is a 17° wide band of $\theta_{2,0}$ ($-32° < \theta_{2,0} < -15°$) for which C is larger than 0.3 C_{max} (Figure 4a). A significant portion (region II in Figure 4a) of this band of relatively strong infragravity response corresponds to a downcoast propagating infragravity wave excited by two upcoast propagating swell components. Thus directionally spread, obliquely incident swells can theoretically drive an infragravity wave field in shallow water with significant upcoast and downcoast traveling components. Although backscattering from topographic irregularities may also yield infragravity waves with an alongshore energy flux opposing the swells, nonlinear wave-wave interaction theory at least qualitatively explains why the

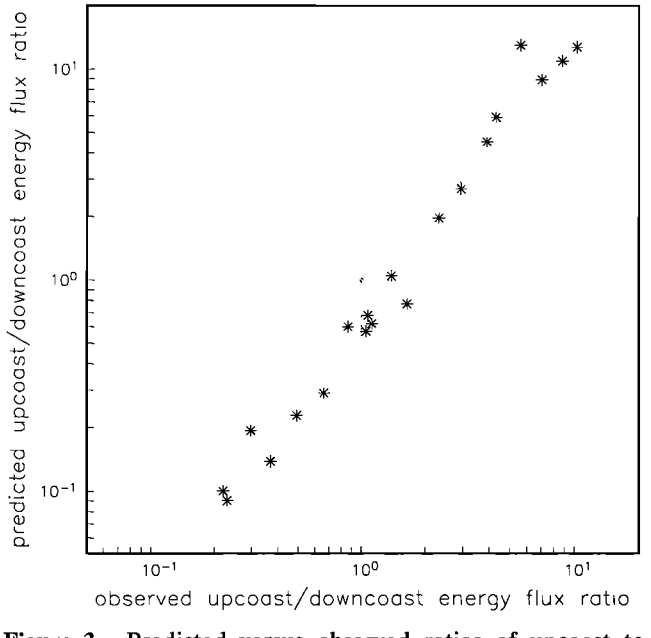

Figure 3. Predicted versus observed ratios of upcoast to downcoast alongshore energy fluxes in the infragravity frequency band ($F_{up}^{IG}/F_{down}^{IG}$) for 20 cases selected to span a wide range of ratios.

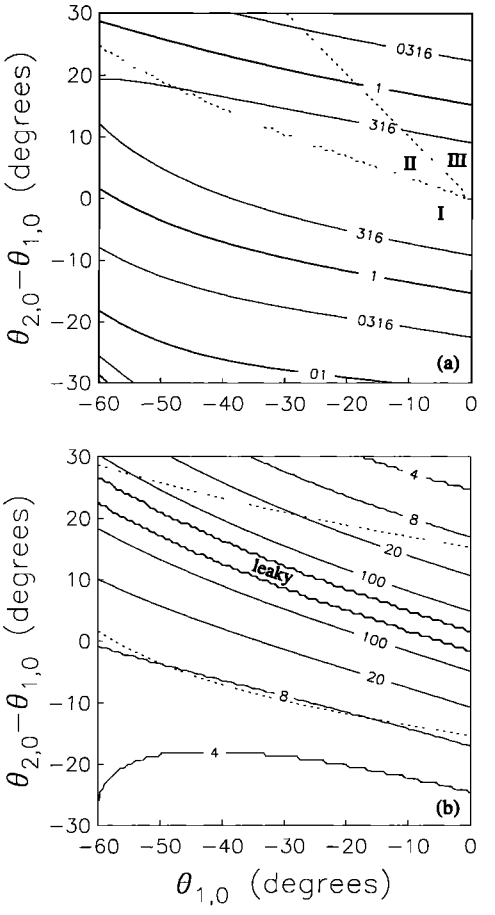

Figure 4. Theoretically predicted properties of a 0.02-Hz free infragravity wave generated by nonlinear interactions between two swell components with frequencies $f_1 = 0.09$ Hz and $f_2 = 0.11$ Hz as a function of the deepwater swell incidence angles $\theta_{1,0}$ and $\theta_{2,0}$ over the range of commonly observed spreading angles ($-30° < \theta_{2,0} - \theta_{1,0} < 30°$). (a) Contours of the relative response C (equation (13), normalized by the maximum value C_{max} for $\theta_{1,0} = \theta_{2,0} = 0$). The regions labeled I, II, and III correspond to upcoast propagation of both incident swell components and the infragravity wave, upcoast propagation of both incident swell components and downcoast propagation of the infragravity wave, and upcoast propagation of one incident swell component and downcoast propagation of the other incident swell component and the infragravity wave, respectively. The dashed line dividing regions I and II is defined by $\sin\theta_{1,0} f_1^2 = \sin\theta_{2,0} f_2^2$ and the dashed line between regions II and III is $\theta_{2,0} = 0$. (b) Contours of the trapping depth h_t (equation (14), units of meters) and leaky domain boundaries (equation (15)). Dashed lines bound the region of significant infragravity response ($C > 0.1C_{max}$).

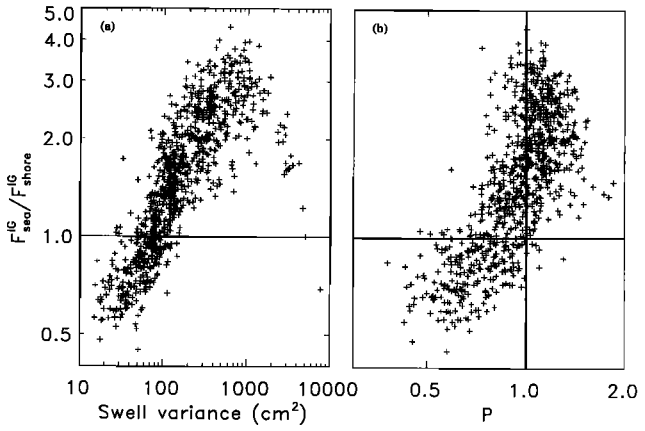

Figure 5. (a) The ratio $F^{IG}_{sea}/F^{IG}_{shore}$ of the seaward to the shoreward component of the cross-shore energy flux in the infragravity frequency band versus the swell variance. (b) $F^{IG}_{sea}/F^{IG}_{shore}$ versus the infragravity directional polarization parameter P (equation 17).

observed ratios of upcoast and downcoast infragravity energy fluxes are closer to unity than the corresponding swell ratios (Figure 1).

3. Cross-Shore Energy Fluxes

3.1. Refractive Trapping

The nonlinear infragravity wave generation model presented in section 2 predicts a directionally broad field of seaward propagating free waves. Whereas infragravity waves propagating directly offshore will radiate to the open ocean, infragravity waves traveling seaward at oblique angles may be refractively trapped on the continental shelf (Figure 2b). On a monotonic, gently sloping shelf (with no alongshelf depth variations) the theoretical trapping depth h_t is obtained by equating the cross-shore wavenumber of the infragravity wave to zero and substituting the alongshore wavenumber and the frequency in the dispersion relation (equation (A1))

$$h_t = \frac{g}{|\sigma_2^2 \sin \theta_{2,0} - \sigma_1^2 \sin \theta_{1,0}|} \cdot \operatorname{arctanh}\left(\frac{(\sigma_2 - \sigma_1)^2}{|\sigma_2^2 \sin \theta_{2,0} - \sigma_1^2 \sin \theta_{1,0}|}\right) \qquad (14)$$

$$|\sigma_2^2 \sin \theta_{2,0} - \sigma_1^2 \sin \theta_{1,0}| > (\sigma_2 - \sigma_1)^2$$

The predicted h_t are less than 100 m for a broad range of interactions with a significant infragravity response (Figure 4b), qualitatively consistent with observed cross-shore variations of infragravity energy [*Elgar et al.*, 1992; *Herbers et al.*, 1995].

Only weak radiation to the open ocean is expected for a shelf that gently slopes to deep water because the theoretical range of swell frequencies and propagation directions that drive "leaky" infragravity waves

$$|\sigma_2^2 \sin \theta_{2,0} - \sigma_1^2 \sin \theta_{1,0}| < (\sigma_2 - \sigma_1)^2 \qquad (15)$$

is very narrow compared with the full range of swell interactions with a significant infragravity response (Figure 4b). If all the infragravity energy radiated from shore is refractively trapped, then (assuming locally forced infragravity energy is negligible well seaward of the surf zone) $F^{IG}_{sea}/F^{IG}_{shore} = 1$, where F^{IG}_{sea} and F^{IG}_{shore} are the seaward and shoreward components of the cross-shore energy flux in the infragravity band

$$F^{IG}_{sea} = -\int_{0.01\ Hz}^{0.04\ Hz} df \int_{\pi/2}^{3\pi/2} d\theta\ \rho g c_g(f) \cos \theta E(f, \theta) \qquad (16a)$$

$$F^{IG}_{shore} = \int_{0.01\ Hz}^{0.04\ Hz} df \int_{-\pi/2}^{\pi/2} d\theta\ \rho g c_g(f) \cos \theta E(f, \theta) \qquad (16b)$$

Estimates of $F^{IG}_{sea}/F^{IG}_{shore}$, obtained from the array measurements with the same technique used to estimate alongshore energy fluxes (section 2) are scattered about the theoretical value of 1 for trapped waves (Figure 5a). However, $F^{IG}_{sea}/F^{IG}_{shore}$ varies systematically between about 0.5 and 5, with the extreme values occurring with relatively low and high swell energy, respectively.

3.2. Radiation and Damping

Both radiation of infragravity waves to deep ocean basins and damping of infragravity waves on the shelf may cause $F^{IG}_{sea}/F^{IG}_{shore} > 1$. Theoretical predictions of leaky infragravity wave energy based on the assumption of deep offshore waters (equation (15)) are inaccurate because typical deepwater infragravity wavelengths (e.g., 16 km for 0.01-Hz waves) exceed the depth of the Atlantic Ocean basin. Additionally, the WKB approximation is invalid on the steep continental slope. Although quantitative predictions of leaky wave energy require much more sophisticated models than (15), the observations suggest that the leaky wave component of the directionally broad infragravity wave fields radiated from shore is small and does not explain the observed high values of $F^{IG}_{sea}/F^{IG}_{shore}$. Estimates of infragravity wave directional properties (e.g., Figure 5b, discussed below) give no indication of a relative increase in energy of shore-normal propagating (i.e., leaky) infragravity waves with increasing $F^{IG}_{sea}/F^{IG}_{shore}$. Furthermore, the propagation of inviscid, small-amplitude long waves across the shelf is governed primarily by linear processes (e.g., refraction, trapping, scattering), and the relative importance of undamped leaky and trapped waves is thus independent of absolute energy levels. In contrast, the observations show a dependence of $F^{IG}_{sea}/F^{IG}_{shore}$ on swell energy levels (Figure 5a).

The values of $F^{IG}_{sea}/F^{IG}_{shore} > 1$ observed during high-energy swell conditions are likely caused by damping of infragravity waves on the shelf. If infragravity waves radiated from shore are significantly damped during propagation from the array to an offshore turning point and back to the array, then $F^{IG}_{sea}/F^{IG}_{shore} > 1$. Although the precise mechanism is unknown, infragravity wave damping by bottom friction is expected to be nonlinear and to depend on the near-bottom orbital velocity field of swell [e.g., *Hasselmann and Collins*, 1968], consistent with the observed increase in $F^{IG}_{sea}/F^{IG}_{shore}$ with increasing swell energy (see *Elgar et al.* [1994] for further discussion). The highest observed values of $F^{IG}_{sea}/F^{IG}_{shore}$ ($\approx$4.5) suggest that the damping is sometimes strong enough to effectively suppress high-mode edge waves.

The ratio $F^{IG}_{sea}/F^{IG}_{shore}$ decreases during the most energetic swell events (Figure 5a; swell variances $> 2 \times 10^3$ cm^2). In these few cases with significant swell wave heights of 2–4 m, the surf zone extended more than 1 km offshore (i.e., close to the array site) and locally forced infragravity waves were readily detectable (Figures 1 and 2 of *Elgar et al.* [1995]; *Her-*

bers et al. [1995]). Although the estimated energy flux ratios must be cautiously interpreted for these extreme events because the linear dispersion relation was assumed, the observed decrease in $F_{sea}^{IG}/F_{shore}^{IG}$ is qualitatively consistent with significant contributions of shoreward propagating forced infragravity waves.

3.3. Remote Sources

Values of $F_{sea}^{IG}/F_{shore}^{IG} < 1$ observed with very low swell energy levels ($<10^2$ cm^2 (Figure 5a)) are clearly not caused by forced wave contributions (bispectral analysis shows that forced waves typically account for less than 1% of the infragravity variance in these cases [*Herbers et al.*, 1995]). Case studies of the directional properties of these shoreward propagating infragravity waves suggest they are arrivals from remote (possibly trans-oceanic) sources [e.g., *Webb et al.*, 1991], rather than the infragravity waves generated at nearby shores more commonly observed on the shelf [*Herbers et al.*, 1995]. If the energy source is offshore and the shoreward propagating infragravity waves are partially dissipated or scattered into trapped modes in the surf zone, then $F_{sea}^{IG}/F_{shore}^{IG} < 1$. The hypothesized importance of remote sources when local swell energy levels are low is consistent with estimates of a directional polarization parameter P

$$P \equiv \frac{\int_{0.01\ \mathrm{Hz}}^{0.04\ \mathrm{Hz}} df \rho g c_g(f) \int_{-\pi}^{\pi} d\theta \mid \sin\theta \mid E(f,\theta)}{\int_{0.01\ \mathrm{Hz}}^{0.04\ \mathrm{Hz}} df \rho g c_g(f) \int_{-\pi}^{\pi} d\theta \mid \cos\theta \mid E(f,\theta)} = \frac{F_{up}^{IG} + F_{down}^{IG}}{F_{sea}^{IG} + F_{shore}^{IG}} \tag{17}$$

Values of $P < 1$ and > 1 correspond to infragravity wave propagation polarized along the cross-shore and alongshore axes, respectively. Infragravity waves arriving from remote sources are refracted toward normal incidence as they propagate across the continental shelf, and thus they have narrow directional spectra in shallow water with $P \ll 1$. Virtually all observations of predominantly shoreward propagating infragravity waves ($F_{sea}^{IG}/F_{shore}^{IG} < 1$ in Figure 5a) do indeed correspond to values of $P < 1$ (lower left quadrant of Figure 5b). The majority of the remaining values of P are roughly scattered about 1, consistent with directionally broad infragravity wave fields radiated from shore.

4. Conclusions

Directional properties of infragravity waves observed a few kilometers from shore depend on the directional properties of incident swell. The alongshore energy fluxes (Figure 1) suggest that although upcoast propagating swell drives mostly upcoast propagating infragravity waves, upcoast propagating swell can have a significant downcoast infragravity response (similar dependencies hold for downcoast traveling swell). These observations are consistent with predictions of a simple spectral model for the generation of infragravity waves by nonlinear interactions of directionally spread, nonbreaking waves shoaling on a monotonically sloping beach with negligible alongshore depth variations. Second-order finite depth wave theory [e.g., *Hasselmann*, 1962] is used to describe the nonlinear forcing of infragravity waves by incident swell, and the forced infragravity waves are released as free waves in the surf zone, reflected from the beach, and radiated seaward (Figure 2a [after *Longuet-Higgins and Stewart*, 1962]). Certain combinations of frequencies and angles of two upcoast propagating swell components drive a downcoast propagating infragravity wave (Figure 4a).

Second-order finite depth theory is singular at the shoreline, and thus cannot be used to predict absolute infragravity energy levels, but the energy distribution in frequency-direction space of infragravity waves radiated from asymptotically shallow water is shown to be a function only of the (deepwater) frequency-directional spectrum of incident swell, independent of the depth where the forced waves are released. Although the effects of wave breaking on the generation and propagation of infragravity waves are neglected, predictions of the relative contributions of upcoast and downcoast propagating waves to the alongshore infragravity energy flux are in good agreement with observations (Figure 3).

The theory also predicts that infragravity waves are typically radiated seaward at oblique angles and refractively trapped on the continental shelf (Figures 2b and 4b), consistent with the observed roughly comparable contributions of seaward and shoreward propagating waves to the cross-shore infragravity energy flux (Figure 5a). However, the observed dominance of seaward propagating infragravity waves during high-energy swell conditions suggests that high-mode edge waves are damped on the shelf [*Elgar et al.*, 1994]. On the other hand, the directionally narrower, predominantly shoreward propagating infragravity waves observed with low-energy swell (Figure 5) shows the importance of infragravity waves arriving from remote sources.

The WKB-continuum approximation used here to model the propagation and trapping of infragravity waves is not applicable to low-mode edge waves, and further work is needed to quantitatively assess the importance of wave breaking to both infragravity wave generation and the subsequent propagation and damping. The qualitative model-data comparisons presented here nonetheless lend strong support for the basic hypothesis that quadratic nonlinear interactions of swell drive free infragravity waves, and they confirm more recent suggestions that the seaward radiated infragravity waves are directionally broad and, to a significant degree, refractively trapped on the continental shelf.

Appendix A: Wavenumbers of Infragravity Waves

Fluxes of energy at infragravity frequencies were estimated from array data (sections 2 and 3; equations (1), (2), and (16)) assuming a wave field composed of statistically independent components with wavenumbers k obeying the linear surface gravity wave dispersion relation

$$\sigma^2 = gk \tanh(kh) \tag{A1}$$

where $\sigma(= 2\pi f)$ is the radian frequency, g is gravity, and h is the water depth. Forced infragravity waves theoretically have higher wavenumbers, but their contribution to the infragravity energy is usually small at this site [*Herbers et al.*, 1995]. Although free infragravity waves are expected to obey the linear dispersion relation, the array analysis is complicated by reflections from the shoreline and offshore caustics. The cross-shore energy variations associated with nodes and antinodes of

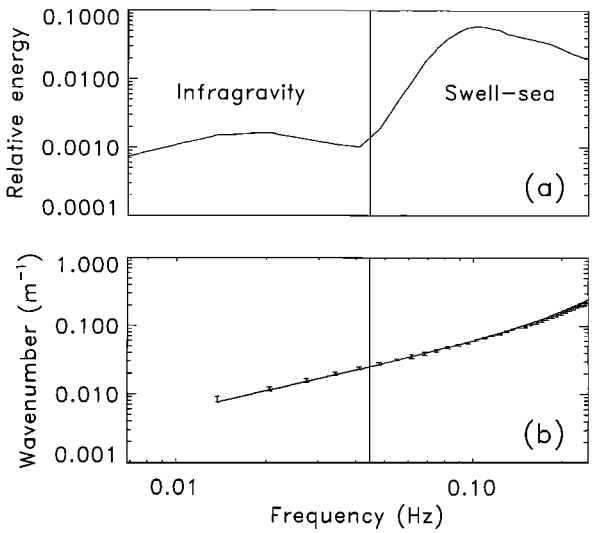

Figure A1. (a) Average shape of sea surface elevation spectra (the average of all depth-corrected bottom pressure spectra, each normalized by the total variance in the infragravity-swell-sea frequency band). (b) Wavenumber magnitude versus frequency. The solid curve indicates the linear dispersion relation (equation (A1)), and the vertical bars represent the average values ± one standard deviation of $k_{\mathrm{rms}}(f)$ estimates (equation (A2)).

standing waves violate the assumption of spatial homogeneity used in most array analysis algorithms. Fortunately, as the distance from shore increases, the frequency separation of nodes and antinodes decreases, and within a sufficiently wide frequency bandwidth the effects of nodes and antinodes cancel and the variance is approximately spatially homogeneous. Free, linear waves do not obey (A1) near caustics, but the observations discussed here were obtained well seaward of the turning points of low-mode edge waves (e.g., modes 0–4 at 0.01 Hz) and a broad spectrum of high-mode edge waves on a gently sloping seabed can be accurately described by a continuous frequency-directional spectrum of waves obeying (A1) [see *Herbers et al.*, 1995]. Thus the effects of both nodal structure and turning points can be neglected in the present array analysis.

To verify that the observed infragravity waves obey the linear dispersion relation, and to confirm that the array analysis is not degraded by standing wave effects or caustics, estimates of a root-mean-square average wavenumber as a function of frequency $k_{\mathrm{rms}}(f)$

$$k_{\mathrm{rms}}(f) \equiv \left[\frac{\int_0^{k_c} dk \int_{-\pi}^{\pi} k \, d\theta \, k^2 E(f, k, \theta)}{\int_0^{k_c} dk \int_{-\pi}^{\pi} k \, d\theta \, E(f, k, \theta)} \right]^{1/2} \tag{A2}$$

with $E(f, k, \theta)$ the frequency-(vector) wavenumber spectrum of seafloor pressure in polar form, were obtained from the array measurements. Waves with wavenumber higher than the cutoff value $k_c \approx 2\pi/h$ are strongly attenuated at the seafloor and not measured by the array. The cross spectrum $H_{pq}(f)$ of a pair of sensors with indices p and q at locations $[x_p, y_p]$ and $[x_q, y_q]$ is related to $E(f, k, \theta)$ by

$$H_{pq}(f) = \int_0^{k_c} dk \int_{-\pi}^{\pi} k \, d\theta \exp\,[ik[(x_p - x_q)\cos\theta + (y_p - y_q)\sin\theta]]E(f, k, \theta) \tag{A3}$$

For sensor separations small compared with the surface wavelength ($[x_p - x_q]k < 1$, $[y_p - y_q]k < 1$), (A3) can be approximated by a truncated expansion

$$H_{pq}(f) \approx \sum_{n=0}^{N_t} \sum_{m=0}^{n} i^n \frac{(x_p - x_q)^{n-m}(y_p - y_q)^m}{(n-m)!m!} \cdot \int_0^{k_c} dk \int_{-\pi}^{\pi} k \, d\theta \, k^n \cos^{n-m}\theta \sin^m\theta E(f, k, \theta) \tag{A4}$$

where N_t is the truncation order.

An estimate of $k_{\mathrm{rms}}(f)$ (equation (A2)) is obtained from a linear combination of the normalized cross spectra

$$\hat{k}^2_{\mathrm{rms}} = \sum_{p=1}^{N_t} \sum_{q=1}^{N_t} \alpha_{pq} \frac{H_{pq}(f)}{[H_{pp}(f)H_{qq}(f)]^{1/2}} \tag{A5}$$

where N_t is the number of sensors in the array. Substitution of (A4) in (A5) gives

$$\hat{k}^2_{\mathrm{rms}} \approx \sum_{n=0}^{N_t} \sum_{m=0}^{n} \sum_{p=1}^{N_t} \sum_{q=1}^{N_t} \alpha_{pq} i^n \frac{(x_p - x_q)^{n-m}(y_p - y_q)^m}{(n-m)!m!} \cdot \frac{\int_0^{k_c} dk \int_{-\pi}^{\pi} k \, d\theta k^n \cos^{n-m}\theta \sin^m\theta E(f, k, \theta)}{\int_0^{k_c} dk \int_{-\pi}^{\pi} k \, d\theta \, E(f, k, \theta)} \tag{A6}$$

Setting the right-hand side of (A6) equal to k^2_{rms} (equation (A2)) yields a linear set of equations for the coefficients α_{pq}

$$\sum_{p=1}^{N_t} \sum_{q=1}^{N_t} \alpha_{pq} i^n \frac{(x_p - x_q)^{n-m}(y_p - y_q)^m}{(n-m)!m!} = 1$$

$$n = 2, \, m = 0 \text{ and } n = 2, \, m = 2$$

$$\sum_{p=1}^{N_t} \sum_{q=1}^{N_t} \alpha_{pq} i^n \frac{(x_p - x_q)^{n-m}(y_p - y_q)^m}{(n-m)!m!} = 0 \tag{A7}$$

$$\text{all other } n, \, m$$

Least squares fit solutions for the α_{pq} were obtained using a singular value decomposition of (A7). To reduce both bias errors introduced by long array lags and the overall computational effort required to process 9 months of data, the calculations were done on a subset of the array lags: 4–23 m for short-wavelength seas (0.15–0.25 Hz), 10–70 m for medium-wavelength swell (0.06–0.15 Hz), and 30–210 m for long-wavelength swell and infragravity waves (0.01–0.06 Hz). In these calculations the number of terms (N_t) kept in the expansion was 8 and the truncation value for the smallest eigenvalue (relative to the largest eigenvalue) was 10^{-4}. Excellent agreement at the overlap frequencies of $\hat{k}_{\mathrm{rms}}$ estimates using

different subarrays confirms the high accuracy of the present wavenumber estimates. Although only estimates of k_{rms} are discussed here, the technique can be applied to any moment of $E(f, k, \theta)$ that can be expressed as a polynomial expansion in $k \cos \theta$, $k \sin \theta$ [*Herbers and Guza*, 1994].

Estimates of $k_{\mathrm{rms}}(f)$ (computed for every 3-hour-long data record) agree well with the linear dispersion relation over a wide frequency band (0.01–0.25 Hz) that includes infragravity waves, swell, and sea (Figure A1). The agreement is best (deviations less than 5%) in the frequency range 0.08–0.14 Hz (Figure A1b) of the dominant swell (Figure A1a). Slight (less than 10%) but systematic deviations of the wavenumber estimates from linear theory at both higher and lower frequencies are consistent with the presence of longer-wavelength forced waves at double-swell frequencies [*Herbers and Guza*, 1994] and shorter-wavelength forced waves at infragravity frequencies [*Herbers et al.*, 1995].

Appendix B: Theoretical Predictions of the Frequency-Directional Spectrum of Infragravity Waves

Frequency-directional spectra of incident swell in 13-m depth were estimated from the array cross spectra with a variational technique [*Herbers and Guza*, 1990; *Herbers et al.*, 1994] and transformed to shallow water with the linear shoaling and refraction relations for a gently (monotonically) sloping seabed $h = h(x)$ with no alongshore depth variations [e.g., *Longuet-Higgins*, 1957; *Le Méhauté and Wang*, 1982]:

$$E_h(f, \theta_h) = \frac{c_{g,13\mathrm{m}} c_{13\mathrm{m}}}{c_{g,h} c_h} E_{13\mathrm{m}}(f, \theta_{13\mathrm{m}}) \qquad \text{(B1a)}$$

$$\sin(\theta_h) = \frac{c_h}{c_{13\mathrm{m}}} \sin(\theta_{13\mathrm{m}}) \qquad \text{(B1b)}$$

where c and c_g denote phase and group velocities and the subscripts 13 m and h indicate values in 13-m depth and at a shoreward location with depth h. Finite depth relationships (e.g., based on (A1)) were used in 13-m depth. The variance of locally forced infragravity waves in depth h, $E_{\mathrm{forced},h}$, is given by

$$E_{\mathrm{forced},h} = \int_{f_1} df_1 \int_{f_2} df_2 \int_{\theta_{1,h}} d\theta_{1,h} \int_{\theta_{2,h}} d\theta_{2,h}\, D^2(f_1, f_2, \theta_{1,h}, \theta_{2,h}) \cdot E_{\mathrm{swell},h}(f_1, \theta_{1,h}) E_{\mathrm{swell},h}(f_2, \theta_{2,h}) \qquad \text{(B2)}$$

where D is the asymptotic shallow-water interaction coefficient (equation (8)) and the integrations are restricted to pairs of swell components with a difference frequency $|f_2 - f_1|$ in the infragravity band. The frequency-directional spectrum of shoreward propagating forced infragravity waves, $E_{\mathrm{forced},h}(f, \theta_h)$, was evaluated numerically by mapping the term inside the (discretized) integral on the right-hand side of (B2) into (f, θ_h) space with the nonlinear interaction rules (for $f_1 < f_2$)

$$f = f_2 - f_1 \qquad \text{(B3a)}$$

$$\theta_h = \arctan\left[\frac{k_{2,h} \sin \theta_{2,h} - k_{1,h} \sin \theta_{1,h}}{k_{2,h} \cos \theta_{2,h} - k_{1,h} \cos \theta_{1,h}}\right] \qquad \text{(B3b)}$$

The forced infragravity waves were released as free waves in depth h and specularly reflected from the beach. Neglecting dissipation, the spectrum of free waves propagating seaward in depth h, $E_{\mathrm{free},h}(f, \theta_h)$, is given by

$$E_{\mathrm{free},h}(f, \theta_h) = E_{\mathrm{forced},h}(f, \pi - \theta_h) \qquad \frac{\pi}{2} < \theta_h < \frac{3\pi}{2} \qquad \text{(B4)}$$

Finally, $E_{\mathrm{free},h}(f, \theta_h)$ is transformed to the 13-m depth array location with (B1). In this WKB-continuum approximation, waves propagating seaward in depth h with oblique angles $|\pi - \theta_h| > \arcsin(c_h/c_{13\mathrm{m}})$ are refractively trapped shoreward of the 13-m depth array and thus do not contribute to $E_{\mathrm{free},13\mathrm{m}}(f, \theta_{13\mathrm{m}})$. Although (B1) is not valid in the vicinity of a caustic, the WKB-continuum approximation yields accurate predictions of the gross directional properties of a broad spectrum of high-mode edge waves on a gently sloping seabed [*Herbers et al.*, 1995]. The predicted absolute spectral levels of seaward radiated free waves are sensitive to the depth h where the forced waves are released, but the relative distribution of $E_{\mathrm{free},13\mathrm{m}}(f, \theta_{13\mathrm{m}})$ in frequency-direction space (used in section 2.3 to calculate ratios of upcoast to downcoast energy fluxes) is independent of h (see section 2.2).

Acknowledgments. This research was supported by the Office of Naval Research (Coastal Dynamics Program, Nonlinear Ocean Waves Accelerated Research Initiative, and Waves in the Ocean Broad Agency Announcement). Staff from the Center for Coastal Studies, Scripps Institution of Oceanography, expertly deployed and maintained the pressure transducer array. Excellent logistical support was provided by the staff of the U.S. Army Corps of Engineers Field Research Facility at Duck, North Carolina. Reviewers provided helpful suggestions.

References

Bowen, A. J., and R. T. Guza, Edge waves and surf beat, *J. Geophys. Res.*, *83*, 1913–1920, 1978.

Elgar, S., T. H. C. Herbers, M. Okihiro, J. Oltman-Shay, and R. T. Guza, Observations of infragravity waves, *J. Geophys. Res.*, *97*, 15,573–15,577, 1992.

Elgar, S., T. H. C. Herbers, and R. T. Guza, Reflection of ocean surface gravity waves from a natural beach, *J. Phys. Oceanogr.*, *24*, 1503–1511, 1994.

Elgar, S., T. H. C. Herbers, V. Chandran, and R. T. Guza, Higher-order spectral analysis of nonlinear ocean surface gravity waves, *J. Geophys. Res.*, *100*, 4977–4983, 1995.

Foda, M. A., and C. C. Mei, Nonlinear excitation of long-trapped waves by a group of short swells, *J. Fluid Mech.*, *111*, 319–345, 1981.

Gallagher, B., Generation of surf beat by non-linear wave interactions, *J. Fluid Mech.*, *49*, 1–20, 1971.

Hasselmann, K., On the non-linear energy transfer in a gravity-wave spectrum, 1, General theory, *J. Fluid Mech.*, *12*, 481–500, 1962.

Hasselmann, K., and J. I. Collins, Spectral dissipation of finite-depth gravity waves due to turbulent bottom friction, *J. Mar. Res.*, *26*, 1–12, 1968.

Herbers, T. H. C., and R. T. Guza, Estimation of directional wave spectra from multicomponent observations, *J. Phys. Oceanogr.*, *20*, 1703–1724, 1990.

Herbers, T. H. C., and R. T. Guza, Nonlinear wave interactions and high-frequency seafloor pressure, *J. Geophys. Res.*, *99*, 10,035–10,048, 1994.

Herbers, T. H. C., R. L. Lowe, and R. T. Guza, Field observations of orbital velocities and pressure in weakly nonlinear surface gravity waves, *J. Fluid Mech.*, *245*, 413–435, 1992.

Herbers, T. H. C., S. Elgar, and R. T. Guza, Infragravity-frequency (0.005–0.05 Hz) motions on the shelf, I, Forced waves, *J. Phys. Oceanogr.*, *24*, 917–927, 1994.

Herbers, T. H. C., S. Elgar, R. T. Guza, and W. C. O'Reilly, Infragravity-frequency (0.005–0.05 Hz) motions on the shelf, II, Free waves, *J. Phys. Oceanogr.*, *25*, 1063–1079, 1995.

Huntley, D. A., R. T. Guza, and E. B. Thornton, Field observations of

surf beat, 1, Progressive edge waves, *J. Geophys. Res.*, *86*, 6451–6466, 1981.

Le Méhauté, B., and J. D. Wang, Wave spectrum changes on a sloped beach, *J. Waterw. Port, Coastal Ocean Eng.*, *108*, 33–47, 1982.

List, J. H., A model for the generation of two-dimensional surf beat, *J. Geophys. Res.*, *97*, 5623–5636, 1992.

Longuet-Higgins, M. S., On the transformation of a continuous spectrum by refraction, *Proc. Cambridge Philos. Soc.*, *53*, 226–229, 1957.

Longuet-Higgins, M. S., and R. W. Stewart, Radiation stress and mass transport in surface gravity waves with application to 'surf beats,' *J. Fluid Mech.*, *13*, 481–504, 1962.

Munk, W. H., Surf beats, *Eos Trans. AGU*, *30*, 849–854, 1949.

Okihiro, M., R. T. Guza, and R. J. Seymour, Bound infragravity waves, *J. Geophys. Res.*, *97*, 11,453–11,469, 1992.

Oltman-Shay, J., and R. T. Guza, Infragravity edge wave observations on two California beaches, *J. Phys. Oceanogr.*, *17*, 644–663, 1987.

Schäffer, H. A., Infragravity waves induced by short-wave groups, *J. Fluid Mech.*, *247*, 551–588, 1993.

Symonds, G., D. A. Huntley, and A. J. Bowen, Two-dimensional surf beat: Long wave generation by a time-varying breakpoint, *J. Geophys. Res.*, *87*, 492–498, 1982.

Tucker, M. J., Surf beats: Sea waves of 1 to 5 minute period, *Proc. R. Soc. London A*, *202*, 565–573, 1950.

Ursell, F., Edge waves on a sloping beach, *Proc. R. Soc. London A*, *214*, 79–97, 1952.

Webb, S. C., X. Zhang, and W. Crawford, Infragravity waves in the deep ocean, *J. Geophys. Res.*, *96*, 2723–2736, 1991.

S. Elgar, School of Electrical Engineering and Computer Science, Washington State University, Pullman, WA 99164-2752.

R. T. Guza, Center for Coastal Studies, 0209, Scripps Institution of Oceanography, University of California, San Diego, La Jolla, CA 92093-0209.

T. H. C. Herbers, Department of Oceanography, Code OC/He, Naval Postgraduate School, Monterey, CA 93943-5123. (e-mail: herbers@oc.nps.navy.mil)

(Received January 10, 1995; revised June 7, 1995;
accepted June 26, 1995.)